Interband electronic transitions and phase transformation of multiferroic Bi1 x La x Fe1 y Ti y O3 ceramics revealed by temperature-dependent spectroscopic ellipsometry

L. P. Xu, L. L. Zhang, P. P. Jiang, J. Yu, Z. H. Duan, Z. G. Hu, Z. Q. Zhu, and J. H. Chu

CrossMark
click for updates

Interband electronic transitions and phase transformation of multiferroic Bi$_{1-x}$La$_x$Fe$_{1-y}$Ti$_y$O$_3$ ceramics revealed by temperature-dependent spectroscopic ellipsometry

L. P. Xu (徐丽萍),[1] L. L. Zhang (张林林),[2] P. P. Jiang (姜鹏鹏),[1] J. Yu (于剑),[2] Z. H. Duan (段志华),[1] Z. G. Hu (胡志高),[1,a)] Z. Q. Zhu (朱自强),[1] and J. H. Chu (褚君浩)[1]

[1]*Key Laboratory of Polar Materials and Devices (MOE), Department of Electronic Engineering, East China Normal University, Shanghai 200241, China*
[2]*Functional Material Research Laboratory, Tongji University, Shanghai 200092, China*

Optical properties and phase transition of Bi$_{1-x}$La$_x$Fe$_{1-y}$Ti$_y$O$_3$ (BLFTO) ceramics with different composition ($0.02 \leq x \leq 0.10$, $0.01 \leq y \leq 0.06$) have been investigated by spectroscopic ellipsometry (SE) in the temperature range of -70–$450\,^\circ$C. The real part of the complex dielectric function ε_1 increases with the temperature. Meanwhile, the imaginary part ε_2 in the low-energy region decreases with the temperature and has an opposite trend in the high-energy side. Four typical interband transitions ($E_a \sim 2.50\,$eV, $E_b \sim 2.70\,$eV, $E_c \sim 3.60\,$eV, and $E_d \sim 4.25\,$eV) can be observed from the second derivative of the complex dielectric functions with aid of the standard critical point model. The critical point (CP) transition becomes broadening and shifts to a lower energy side as La and Ti compositions increase. Moreover, the CP transition energies show a red-shift trend with increasing the temperature until $320\,^\circ$C, due to the lattice thermal expansion and electron-phonon interaction. The typical interband transitions and partial spectral weight present anomalies in the proximity of antiferromagnetic transition owing to the coupling between magnetic and ferroelectric order parameters and spin-lattice coupling for BLFTO multiferroic materials. It was found that the Néel temperature of BLFTO ceramics decreases from 364 to $349\,^\circ$C with increasing doping composition of La and Ti elements. These phenomena can be attributed to the modification of electronic structure and magnetic order because the differences of electronegativity and ionic radii between Bi and La, Fe and Ti induce the variations on the bond angle and bond length between cations and anions. Moreover, the substitution for magnetic Fe^{3+} ions with nonmagnetic Ti^{4+} ions can reduce the exchange interaction between adjacent magnetic moments. Therefore, SE technique can be sensitive for detecting the phase/structural transitions of multiferroic oxides. © *2013 AIP Publishing LLC*. [http://dx.doi.org/10.1063/1.4851795]

I. INTRODUCTION

Multiferroic materials exhibiting at least both magnetic and ferroelectric orders are known since the 1960s.[1,2] During the last several years, a huge interest in multiferroic materials has been regained due to intriguing physical properties and their potential applications for new spintronics and opto-electronics devices.[1,3] BiFeO$_3$ (BFO) is one of the widely investigated and promising candidates among the multiferroic materials because both ferroelectric and magnetic orders can coexist at room temperature (RT).[4] BFO is antiferromagnetic below Néel temperature of $T_N = 370\,^\circ$C, and ferroelectric below Curie temperature of $T_C = 830\,^\circ$C.[5] BFO can present a strong coupling between the electric and magnetic order parameters, called the magnetoelectric (ME) effect, which makes it a potential candidate for applications to microelectronic and optoelectronic devices, such as actuators, transducers, and storage prototypes.[6–8]

As we know, BFO ceramics possess a rhombohedrally distorted perovskite structure with space point group $R3c$ at RT. The Bi^{3+} and Fe^{3+} cations are displaced from their centrosymmetric positions along the [111]$_{pseudocubic}$ threefold polar axis, leading to a spontaneous polarization. Adjacent oxygen octahedra FeO$_6$ rotates around the [111]$_{pseudocubic}$ direction, corresponding to (a^- a^- a^-) tilt system in Glazer's notation.[1,9] The Fe^{3+} magnetic moments are coupled antiferromagnetically between adjacent planes and ferromagnetically within (111)$_{pseudocubic}$ planes.[9] However, BFO has a 62 nm long cycloidal spiral structure, which is incommensurate with the lattice, cancels out the macroscopic magnetization and suppresses the observation of the linear magnetoelectric effect.[8,10,11] In addition to inhomogeneous magnetic spin structure, there are still other obstacles to be overcome before its applications, such as high leakage current, small spontaneous polarization (P_s), remnant polarization (P_r),[12,13] high coercive field,[14] and ferroelectric unreliability.[15,16] Doping engineering in BFO has been proved to be effective in solving these problems mentioned above. Lanthanum (La) and titanium (Ti) codoped BFO shows enhanced ferromagnetic properties, improved ferroelectric properties and reduced leakage current. This is because the codoping of La and Ti could modify the long-range cycloidal spiral structure, resulting in a homogeneous spin structure.

a)Author to whom correspondence should be addressed. Electronic mail: zghu@ee.ecnu.edu.cn. Tel.: +86-21-54345150. Fax: +86-21-54345119.

Furthermore, the substitution of Ti^{4+} for Fe^{3+} reduces the oxygen (O) vacancies significantly due to the requirements of charge compensation. In addition, the hybridization between Ti 3d and O 2p states is essential for stabilizing the ferroelectric distortion.[4,6,9,16,17] Nevertheless, there are only few reports on La and Ti codoped BFO, which are focused on the effects about ferroelectric, dielectric, magnetic, and impedance behavior.[4,18,19]

On the other hand, optical properties of materials play an important role in understanding the electronic structures and physical characteristics,[20] which could be critical for developing the novel spintronics and optoelectronics devices. One can expect that electronic transitions are related to the crystal structure, which can be affected by the doping and external fields (i.e., temperature and pressure).[21–23] However, as compared to electrical and magnetic studies, the intrinsic mechanisms of optical properties, such as the complex dielectric functions and interband electronic transitions, and their temperature evolution for La and/or Ti codoped BFO system have not been presented up to date. Spectroscopic ellipsometry (SE) is a sensitive measurement technique that uses polarized light to characterize films, surfaces, and material microstructure. SE is a highly suitable method of determining optical functions over a wide range of photon energy. Recently, a large amount of thermo-ellipsometric studies for phase transition detection have been reported.[24–27] It is because the phase transitions can be accompanied by changes of refractive index, the optical band gap and various parameters calculated from ellipsometric data. Compared to conventional methods of measuring phase transition, such as nuclear magnetic resonance (NMR), nuclear quadrupole, resonance (NQR),[28] beta-detected NMR (or NQR),[29] and second harmonic generation (SHG),[30] SE studies allow us to detect phase transition in an effective and non-destructive way, which is very important for film and crystal engineering.[31] Moreover, the relationship between the electronic structure and phase transition can be found for BFO multiferroic system. Correspondingly, it may open an effective method to study phase transformation of ferroelectric oxides.

In this article, the complex dielectric functions of $Bi_{1-x}La_xFe_{1-y}Ti_yO_3$ (BLFTO) ceramics and their temperature dependence have been investigated by SE. The spectra show distinct electronic transition patterns together with charge-transfer transitions. Using the standard line-shape analysis, the transition energies can be reasonably obtained. Moreover, composition dependence of T_N and La/Ti codoping effects have been discussed in detail.

II. EXPERIMENTAL DETAILS

$Bi_{1-x}La_xFe_{1-y}Ti_yO_3$ ceramics were made by a traditional solid state reaction method with Bi_2O_3 (Alfa Aesar 99%), Fe_2O_3 (Alfa Aesar 99.945%), La_2O_3 (Sinochemical 99.99%), and TiO_2 (Acrōs 98%) as raw materials. Stoichiometric mixture of the starting oxide powders were ball-milled for 24 h with stabilized ZrO_2 media and then calcined at 680 °C for 5 h. In order to prevent off-stoichiometry due to Bi_2O_3 adhering on milling media, surfactant was added into slurry before the start of milling. After calcination, powders were reground,

granulated, and pressed uniaxially into green pellets under 250 MPa. These pellets were sintered at 890 °C depending on compositions with a program of heating in a 2 °C/min rate from room temperature to 600 °C and soaking for 2 h to debinder, heating further in 3 °C/min to sintering temperature and soaking for 2 h, then stopping heating and cooling with oven. To remove the surface overlayer artifacts in analyzing the SE data, all BLFTO wafers were double-side polished with a mechanical polishing progress. This progress consists of three steps: coarse grinding, fine grinding, and polishing. Then, the ceramics were rigorously cleaned in pure ethanol with an ultrasonic bath and rinsed several times by deionized water for spectral measurements.

The phase and crystal structure of $Bi_{1-x}La_xFe_{1-y}Ti_yO_3$ ceramics were determined by X-ray diffraction (XRD) using Cu $K\alpha$ radiation (D/MAX-2550 V, Rigaku Co.). To investigate the complex dielectric functions of BLFTO ceramics and temperature evolution of interband transitions, a variable-angle near-infrared-ultraviolet SE (V-VASE, J. A. Woollam) was applied in the range of photon energy of $E_{h\nu} = 1.1$–6.0 eV (wavelength $\lambda \sim 1100$–200 nm). The ellipsometric angles Ψ and Δ were measured in the reflection mode at an incident angle of 70°. To carry out the variable-temperature experiment, the ceramics are mounted into an Instec cell from -70 to 450 °C with a precision of about ± 1 °C, Note that the window corrections are included during the measurement process.

Generally, SE measures the change ratio in the polarization of light reflected from the sample surface, which is written as:[32]

$$\rho = R_p/R_s = \tan\Psi e^{i\Delta}. \quad (1)$$

Here, the complex reflection coefficients R_p and R_s are for the parallel (p) and perpendicular (s) polarized light, respectively. ρ is a complex number that contains phase information. The complex dielectric function ε as a function of ellipsometric parameters Ψ and Δ is given by:[32]

$$\varepsilon = \varepsilon_1 + i\varepsilon_2 = \sin^2\Phi\left[1 + \left(\frac{1-\rho}{1+\rho}\right)^2\tan^2\Phi\right], \quad (2)$$

where Φ denotes the angle of incidence, ε_1 and ε_2 indicate the real and imaginary parts of the complex dielectric function, respectively. The complex dielectric functions for BLFTO ceramics are obtained by the above two-phase model analysis, which consists of the ambient and BLFTO bulk. The root-mean-square surface roughness is 2.66, 1.52, 1.37, and 2.71 nm for the La concentration at $x = 0.02, 0.05, 0.08$, and 0.10, respectively. So the roughness of BLFTO ceramics can be neglected during the analysis.

III. RESULTS AND DISCUSSION

A. Crystal structure

Fig. 1 presents XRD patterns of the BLFTO ceramics recorded at RT. The diffraction patterns with a space group of $R3c$ are very similar with that of parent BFO phase. In
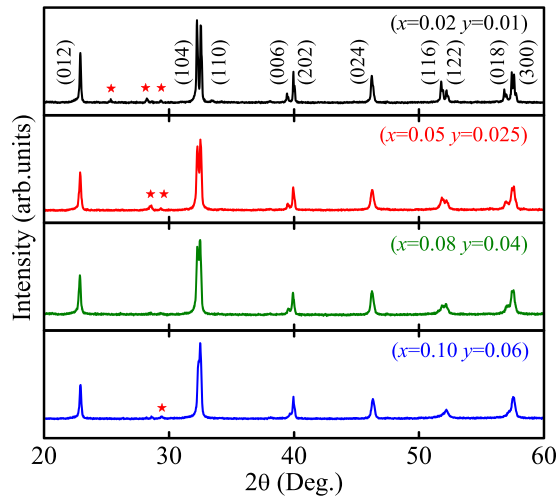
FIG. 1. The XRD patterns of $Bi_{1-x}La_xFe_{1-y}Ti_yO_3$ ceramics at room temperature. The pentacles indicate the diffraction peaks from the $Bi_2Fe_4O_9$ phase.

addition, a parasitic phase $Bi_2Fe_4O_9$ can be observed. The impurity phase may be formed during the high-temperature sintering. Moreover, the intensity of the (104), (006), and (018) diffraction peaks become weaker and the doubly spilt peaks in the 2θ ranges of 31°–33°, 39°–41°, and 51°–53° partially merge to form broadening peaks as La and Ti compositions increase. The differences suggest that the rhombohedral distortion was inhibited by the La and Ti substitution. These observations agree well with those reported for La-doped BFO ceramics.[8,33]

B. The complex dielectric functions

The complex dielectric functions are powerful experimental data, from which the electronic band structure can be observed.[22] The structures observed from the ε spectra of BLFTO are attributed to E_a, E_b, E_c, and E_d electronic transitions (critical points). The real and imaginary parts of the complex dielectric functions between 1.1 and 6.0 eV at three selected temperatures are shown in Fig. 2. For BLFTO
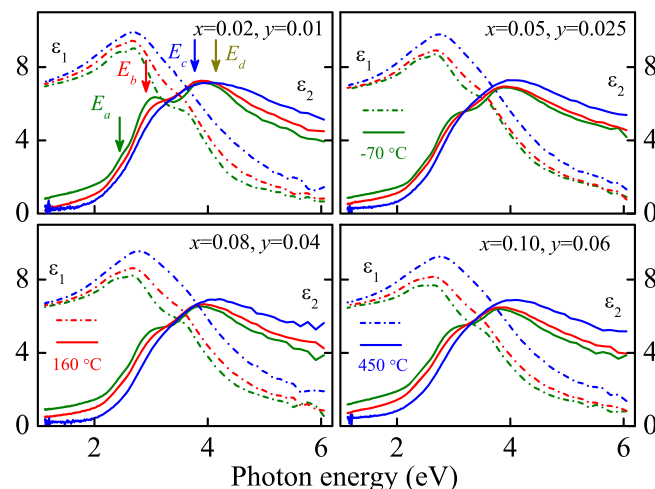
$(x = 0.02, y = 0.01)$, the parameter ε_1 (the real part) is close to 7.2 and ε_2 (the imaginary part) approaches zero in the low-energy region. The parameter ε_1 increases with the temperature in all range of photon energy recorded. Meanwhile, the parameter ε_2 in the low-energy region decreases with the temperature and has an opposite trend in the high-energy side. The complex dielectric functions ε of all BLFTO ceramics have the similar variation tend with the temperature. On the other hand, four typical interband electronic transitions can be unambiguously observed. The four main structures (E_a, E_b, E_c, and E_d) shift to a lower energy side and become broadening with increasing the temperature.

The assignments of the critical points for BLFTO ceramics with the doping are presented in Fig. 3. The critical point transitions become broadening and show a red-shift trend as the La and Ti compositions increase. The effect can be explained by different electronegativities of Bi, La, Fe, and Ti: the electronegativities of Bi and La are 2.02 and 1.83 on the Pauling scale, respectively. The values of electronegativity for La and Ti are 1.1 and 1.54, respectively. The covalent bond strength is directly relative to the differences in electronegativity of the involved atoms. The reduction of four electronic transition energies can be attributed to decreasing in covalent bond strength,[34] which suggests that the codopants have remarkable influence on electronic band structures.

C. Interband electronic transitions in $Bi_{1-x}La_xFe_{1-y}Ti_yO_3$

To further clarify the electronic structure, the second derivative of the complex dielectric functions ($d^2\varepsilon/dE^2$) is numerically calculated. A line-shape analysis with standard critical point (SCP) was performed, which is a common approach in SE measurement and has been applied to semiconductor and ferroelectric materials.[27,35,36] The standard line-shape expression can be written as the following:[36]

$$\frac{d^2\varepsilon}{dE^2} = \begin{cases} n(n-1)A_m e^{i\phi_m}(E - E_m + i\Gamma)^{n-2}, & n \neq 0 \\ A_m e^{i\phi_m}(E - E_m + i\Gamma_m)^{-2}, & n = 0, \end{cases} \quad (3)$$
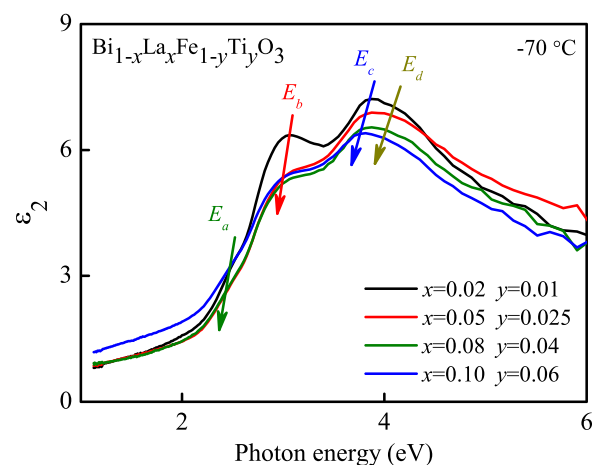

FIG. 2. The real (ε_1) and imaginary (ε_2) parts of the complex dielectric functions for BLFTO measured at −70, 160, and 450 °C, respectively. The arrows indicate four typical interband electronic transitions.

FIG. 3. The imaginary part of the complex dielectric functions for BLFTO ceramics with different La and Ti compositions at −70 °C. The decreasing trend of critical point energies with increasing La and Ti contents is shown by the arrows.

where m expresses the mth oscillator, A_m, E_m, Γ_m, and ϕ_m in order are the amplitude, the threshold energy, the broadening parameter, and the phase angle, respectively. The exponent n has the values of -1, $-\frac{1}{2}$, 0, and $+\frac{1}{2}$ for excitonic, one-dimensional (1D), 2D, and 3D critical points (CPs), respectively. Here, both real and imaginary parts were fitted simultaneously.

The second derivatives of ε_1 and ε_2 for all BLFTO ceramics at different temperature calculated from experimental data (dotted) and the corresponding best-fit curves (solid lines) are shown in Fig. 4. The critical point positions are indicated by the arrows and labeled as E_a, E_b, E_c, and E_d in the order of increasing the photon energy. For clarity, the parameter values of SCP model at several typical temperatures are summarized in Table I. The error bars are less than 0.1 for the parameter A_m ($m = 0$, 1, 2, 3). Correspondingly, the error bars for the angle phase ϕ_m ($m = 0$, 1, 2, 3) and broadening Γ_m ($m = 0$, 1, 2, 3) are less than $0.2°$ and $0.01\,\text{eV}$, respectively. For BLFTO ($x = 0.02$, $y = 0.01$) ceramic at $-70\,°\text{C}$, four critical point energies are estimated to be 2.52 ± 0.02, 2.78 ± 0.01, 3.67 ± 0.03, and $4.29 \pm 0.06\,\text{eV}$, respectively. The phase angle values (ϕ_m) of four critical points in all temperatures are located between $0°$ and $90°$, conforming the excitonic metamorphism of critical-point line shapes.[36] Actually, the deviation of phase angle ϕ_m between -70 and $400\,°\text{C}$ is less than $2°$ from Table I. The angle is almost kept as a constant with increasing the temperature, indicating the reliability of the lineshape chosen for those critical points. Four interband transition energies show

a red-shift trend with increasing doping compositions of La and Ti, which agrees well with the previous discussions.

The physical origin of four critical points could be explained by comparing theoretical electronic band structures. For BFO with $R3c$ rhombohedral structure, the top of the valence band (VB) consists of O $2p$ mixed with Fe $3d$ states. The Fe $3d$ states continue in the conduction band (CB) with some oxygen hybridization and are divided into t_{2g} and e_g manifolds, then the Bi $6p$ states follow.[37–40] Due to the hybridization between O $2p$ and Fe $3d$ states, the electronic properties of BFO are mainly determined by both the charge-transfer transitions from the occupied O $2p$ to unoccupied Fe $3d$ states, and the d-d transition between Fe $3d$ valence and conduction bands. The theoretical results suggested that the substitution of La for Fe cannot contribute much since La $5d$ states are higher than Bi $6p$ states in the conduction band.[34] As to the substitution of Ti in B-cation, the lowest unoccupied energy level of Ti^{4+} ion is d states, which tend to hybridize with O $2p$ states.[16] Therefore, the origin of the structure E_a ($\sim 2.52\,\text{eV}$) has been suggested as a dipole-forbidden p-d transition.[2] The structure E_b ($\sim 2.76\,\text{eV}$) has been assigned to the transitions from either the occupied O $2p$ to unoccupied B-cation metal $3d$ states or the d-d transition between the $3d$ valence and conduction bands.[35,37] The parameters E_c ($\sim 3.67\,\text{eV}$) and E_d ($\sim 4.28\,\text{eV}$) can be ascribed to the transitions from O $2p$ valence band to B-cation metal $3d$ or Bi $6p$ conduction band.[35,37] Note that the obvious discrepancy between the spectra recorded at $-70\,°\text{C}$ and $320\,°\text{C}$ indicates that the temperature has a remarkable influence on electronic band structures of BLFTO ceramics.

To shed light on the variation of the critical point energies, temperature dependence of the critical point energies for BLFTO ceramics is depicted in Fig. 5. The E_a, E_b, E_c, and E_d values decrease as the temperature increases from -70 to $320\,°\text{C}$. It is widely recognized that electron-phonon interaction and lattice thermal expansion are responsible for the red-shift of the critical point energies with the temperature. Due to the expansion of lattice, the lattice constant of BLFTO ceramics can be changed. The variation in the lattice constant modifies the electronic band structure, which further moves the conduction band downward and the valence band upward.[41] The anomalies of the critical point energies are in consistent with antiferromagnetic transition for all compositions, indicating an intimate connection between antiferromagnetic transition and electronic band structure. The result is in agreement with the earlier observation from BFO.[1] In BFO, the lattice parameters and bond length of Fe-O and Bi-O bonds have a jump in the proximity of the antiferromagnetic transition due to the strong spin-lattice coupling. All these changes mentioned above can lead to the modification of electronic band structure, which further results in the anomalies of the critical point energies. Thus, it confirms that SE is a powerful method to detect the phase transition.
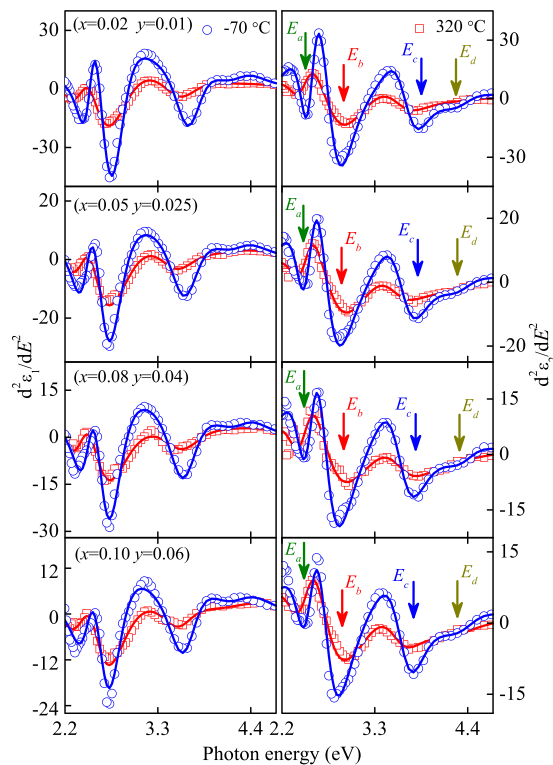

FIG. 4. Experimental (dots) and the best-fit (solid lines) second derivatives of ε_1 and ε_2 at different temperature for BLFTO ceramics, respectively. Note that energies of each critical point are indicated by the arrows and labeled as E_a, E_b, E_c, and E_d in the order of increasing photon energy.

D. Antiferromagnetic transition in $Bi_{1-x}La_xFe_{1-y}Ti_yO_3$

As previously discussed, the anomalies of the interband transitions energies are concerned with antiferromagnetic transition. The magnetic structure arranges itself continuously

TABLE I. The parameters of SCP model for Bi$_{1-x}$La$_x$Fe$_{1-y}$Ti$_y$O$_3$ ceramics are extracted from the best-fit second derivative of the complex dielectric functions (Figure 4) at −70, 200, and 400 °C, respectively. Note that the error bars are presented in parenthesis.

| Samples Temperature (°C)		x = 0.02, y = 0.01			x = 0.05, y = 0.025			x = 0.08, y = 0.04			x = 0.1, y = 0.06		
		−70	200	400	−70	200	400	−70	200	400	−70	200	400
E_a	A_0	0.95 (0.01)	0.82 (0.02)	0.31 (0.03)	1.07 (0.02)	0.99 (0.01)	0.35 (0.01)	1.06 (0.02)	1.04 (0.04)	0.26 (0.03)	0.95 (0.01)	0.91 (0.03)	0.24 (0.04)
	ϕ_0 (deg)	40.6 (0.08)	40.7 (0.12)	40.9 (0.07)	40.4 (0.06)	40.7 (0.10)	41.6 (0.13)	40.5 (0.09)	40.3 (0.11)	41.1 (0.05)	40.7 (0.08)	41.3 (0.12)	41.4 (0.16)
	E_0 (eV)	2.52 (0.02)	2.47 (0.01)	2.42 (0.05)	2.49 (0.02)	2.46 (0.03)	2.41 (0.06)	2.48 (0.02)	2.43 (0.02)	2.41 (0.05)	2.47 (0.02)	2.45 (0.02)	2.43 (0.05)
	Γ_0 (eV)	0.18 (0.002)	0.21 (0.003)	0.23 (0.005)	0.23 (0.003)	0.28 (0.004)	0.21 (0.004)	0.24 (0.004)	0.29 (0.006)	0.25 (0.005)	0.25 (0.005)	0.29 (0.002)	0.24 (0.008)
E_b	A_1	5.00 (0.03)	5.32 (0.05)	6.91 (0.06)	4.77 (0.02)	5.47 (0.03)	6.34 (0.06)	4.37 (0.03)	4.99 (0.05)	6.68 (0.04)	3.44 (0.01)	5.42 (0.06)	6.47 (0.08)
	ϕ_1 (deg)	38.8 (0.07)	38.8 (0.05)	38.7 (0.09)	38.4 (0.06)	38.4 (0.09)	38.8 (0.11)	38.5 (0.09)	38.3 (0.10)	38.5 (0.07)	38.5 (0.09)	38.4 (0.13)	38.6 (0.14)
	E_1 (eV)	2.78 (0.01)	2.76 (0.01)	2.79 (0.02)	2.71 (0.04)	2.67 (0.01)	2.70 (0.04)	2.69 (0.02)	2.65 (0.03)	2.73 (0.03)	2.67 (0.01)	2.61 (0.03)	2.75 (0.05)
	Γ_1 (eV)	0.35 (0.001)	0.48 (0.002)	0.62 (0.005)	0.38 (0.002)	0.49 (0.004)	0.65 (0.007)	0.37 (0.003)	0.48 (0.005)	0.69 (0.005)	0.37 (0.003)	0.51 (0.004)	0.70 (0.007)
E_c	A_2	1.89 (0.03)	1.19 (0.02)	1.15 (0.01)	1.66 (0.02)	1.53 (0.03)	1.33 (0.05)	1.69 (0.02)	0.89 (0.01)	1.10 (0.0.4)	1.25 (0.02)	0.87 (0.01)	0.58 (0.03)
	ϕ_2 (deg)	38.7 (0.07)	38.6 (0.08)	38.5 (0.18)	38.7 (0.09)	38.7 (0.08)	38.6 (0.08)	38.7 (0.15)	38.4 (0.08)	37.9 (0.16)	39.0 (0.18)	39.3 (0.15)	38.0 (0.07)
	E_2 (eV)	3.67 (0.03)	3.58 (0.02)	3.53 (0.2)	3.63 (0.02)	3.58 (0.02)	3.55 (0.07)	3.61 (0.02)	3.52 (0.05)	3.47 (0.08)	3.59 (0.02)	3.56 (0.04)	3.46 (0.07)
	Γ_2 (eV)	0.33 (0.003)	0.37 (0.005)	0.46 (0.007)	0.37 (0.002)	0.45 (0.005)	0.49 (0.003)	0.36 (0.007)	0.37 (0.005)	0.48 (0.004)	0.36 (0.002)	0.39 (0.001)	0.39 (0.004)
E_d	A_3	0.62 (0.01)	1.25 (0.03)	1.51 (0.04)	0.42 (0.01)	0.75 (0.02)	1.35 (0.04)	0.67 (0.02)	1.78 (0.04)	1.74 (0.03)	0.67 (0.02)	1.66 (0.03)	2.09 (0.05)
	ϕ_3 (deg)	40.5 (0.18)	40.1 (0.15)	39.0 (0.06)	40.5 (0.17)	40.5 (0.16)	39.6 (0.05)	40.8 (0.07)	40.4 (0.08)	41.3 (0.19)	40.9 (0.08)	40.7 (0.07)	40.4 (0.11)
	E_3 (eV)	4.29 (0.06)	4.16 (0.07)	4.03 (0.4)	4.27 (0.09)	4.23 (0.04)	4.11 (0.2)	4.25 (0.1)	4.17 (0.2)	4.05 (0.3)	4.22 (0.05)	4.19 (0.08)	4.15 (0.3)
	Γ_3 (eV)	0.41 (0.001)	0.63 (0.003)	0.81 (0.006)	0.41 (0.002)	0.64 (0.005)	0.76 (0.008)	0.39 (0.001)	0.80 (0.003)	0.84 (0.004)	0.49 (0.002)	0.85 (0.003)	0.91 (0.002)
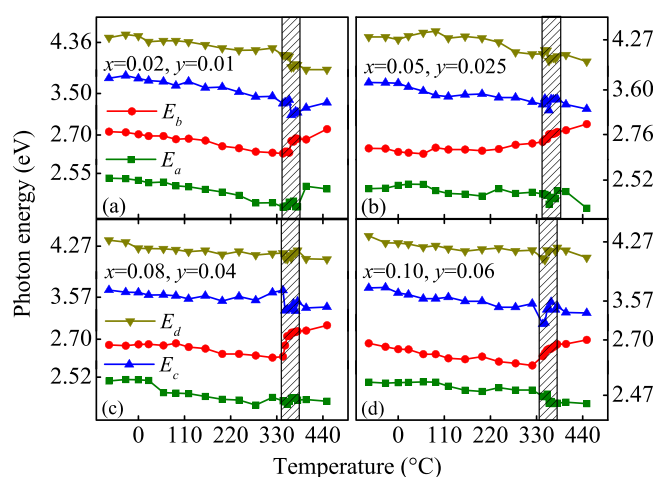
FIG. 5. Temperature dependence of the critical point energies for BLFTO ceramics. Note that the shadow parts present the anomalies.

in a temperature region, which is indicated by the shadow pattern in Fig. 5. To quantitatively extract Néel temperature T_N, the first derivative of the critical point energies with the temperature for all BLFTO ceramics are shown in Fig. 6. It is worth noting that the temperature coefficients of interband transitions energies vary progressively lower than 320 °C, while the dramatic change appears beyond 320 °C. Antiferromagnetic transition occurs at the dip or peak, where all four interband transitions energies have a kink pattern. Thus, the Néel temperature T_N can be uniquely assigned.

As a kind of materials, BLFTO has a similar structure to BFO. The Fe magnetic moments are coupled ferromagnetically within $(111)_{pseudocubic}$ planes and antiferromagnetically between adjacent planes.[9] The weak ferromagnetism is intimately concerned with the symmetry of the system.[42] Owing to tilting of BO_6 octahedra, the angle of Fe-O-Fe chains is not 180°, which results in canted spin arrangements. Since the exchange interaction comes up via these Fe-O-Fe chains, the canted spin arrangements further lead to antiferromagnetism with the weak ferromagnetism. However, BFO has a
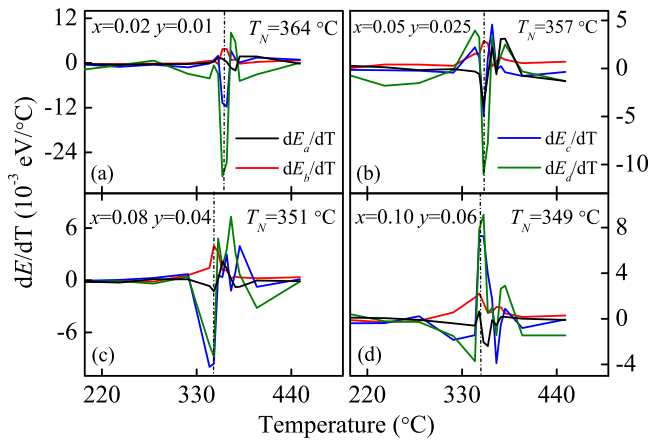
FIG. 6. The first derivative of the critical-point energies with the temperature for BLFTO ceramics. The dashed lines denote the determination of Néel temperature T_N.
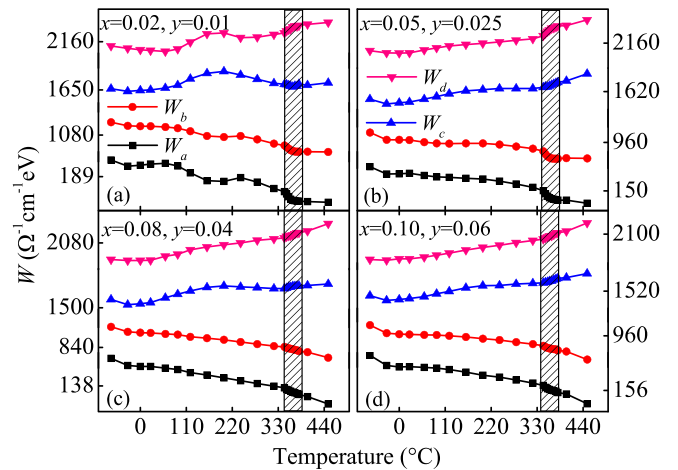

FIG. 7. Temperature dependence of partial spectral weights in different energy regions for BLFTO ceramics. Partial spectral weights in the photon energy regions of 2.4–2.6 eV, 2.7–3.2 eV, 3.5–4.0 eV, and 4.0–4.5 eV are labeled as W_a, W_b, W_c, and W_d, respectively. Note that the shadow parts indicate the anomalies.

G-antiferromagnetic arrangement (G-AF), in which each magnetic atom is surrounded by six antiferromagnetically neighbors (for an ideal cubic perovskite-type structure).[8] The G-AF arrangements show a spiral cycloidal spin arrangement, where there is a periodicity of 62 nm at RT, canceling out the macroscopic magnetization in bulks. The spiral spin structure can be effectively suppressed by the doping because the balance between the antiparallel sublattice magnetization of Fe^{3+} can be broken down and the nature of canted antiferromagnetic sublattices does not be changed by doping at the same time.[43] Therefore, BLFTO has similar canted antiferromagnetic sublattices and magnetic ordering. Due to the thermal disturbance with increasing the temperature, the impact of thermal motion is larger than that from the exchange interaction between adjacent magnetic moments at T_N, which breaks down the balance between the antiparallel sublattice magnetization of Fe^{3+} and gives rise to spin re-orientation of magnetic moments. More experimental and theoretical work is necessary to identify the physical mechanisms of antiferromagnetic transition.

It should be noted that all four interband transitions are related to Fe/Ti 3d states, which indicates that interband transitions are sensitive to Fe/Ti 3d states. It is concluded that antiferromagnetic transition has a remarkable influence on interband transitions. The anomalies in the interband transition energies in the vicinity of T_N may be related to the coupling between magnetic and ferroelectric order parameters for multiferroic materials. Thus, temperature dependence of the ferroelectric order parameter cannot be ignored when the antiferromagnetic transition occurs. It is suggested that the antiferromagnetic transition takes place accompanying with lattice instabilities.[44]

To further discern the variation of electronic structure with the temperature, the partial spectral weights in the photon energy ranges of 2.4–2.6 eV, 2.7–3.2 eV, 3.5–4.0 eV, and 4.0–4.5 eV were analyzed. The partial spectral weight integral (W), which can describe the effective number of electrons excited by photons at a given energy, is defined as $W = \int_{E_1}^{E_2} \sigma_1(E)dE$, where E_1 and E_2 indicate lower and upper boundary of the energy region, respectively.[45] In Fig. 7, the parameter W in the above four energy regions is labeled as

W_a, W_b, W_c, and W_d, respectively. The W_a and W_b values shrink with the temperature and decrease rapidly around T_N. The phenomena accord with the downtrend of ε_2 in the low-energy region from Fig. 2, which can be ascribed to the fact that the electron transitions are primarily caused by thermal activation with increasing the temperature. The parameters W_c and W_d increase monotonically with the temperature due to the strong absorption in high-energy region with the temperature, which show anomalies in the vicinity of T_N. Overall, the temperature dependence of W shows the striking similarities from different samples. Four energy regions mentioned above are dominated by optical transitions between O 2p and Fe/Ti 3d states, thereinto, Fe/Ti 3d states split into t_{2g} and e_g states. Thus, the partial spectral weight integral should be sensitive to specific orbital configurations and orderings.[46,47] The anomalies of W in four energy regions indicate that changes of the electronic structure occur prior to antiferromagnetic transition, which agrees well with the previous discussions from Fig. 5. It suggests the interplay between spin, charge, and orbital correlations through the change of the electron effective Fe/Ti 3d-O 2p and Fe/Ti d-d hopping integrals.

E. Composition dependence of Néel temperature T_N

Fig. 8 shows the composition dependence of Néel temperature T_N. With increasing doping compositions of La and Ti, the Néel temperature decreases from 364 to 349 °C. Lin *et al.*[33] also observed the variation tendency of Néel temperature in La-doped BFO compound by differential scanning calorimetry measurements. To shed light on the variation trend of Néel temperature, the influence of doping on microstructure should be taken into consideration. The instability in ABO_3 perovskite structure is partly involved in the lattice mismatch between the cations. The mismatch is conveniently quantified in the light of the empirical Goldsmith tolerance factor t. The formula for t is $t = (r_A + r_O)/\sqrt{2}(r_B + r_O)$, where r_A, r_B, and r_O are the ionic radii of the A, B, and O ions, respectively. The calculated t for BFO is 0.96.[39] It is
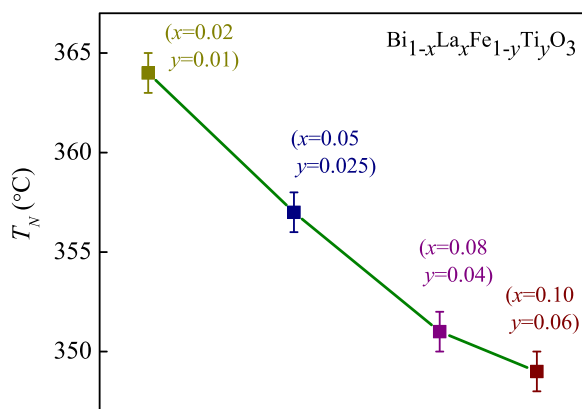
FIG. 8. Composition dependence of Néel temperature T_N for BLFTO ceramics.

less than one, which corresponds to high stability of the cubic perovskite structure. To minimize the mismatch and gain stability, the cooperative FeO_6 octahedra rotates along the [111] direction, resulting in a lattice distortion. According to La and Ti-codoped in BFO, the lattice mismatch can be ameliorated because the radius of La^{3+} is larger than Bi^{3+} (La^{3+}: 1.061 Å, Bi^{3+}: 1.03 Å), while the radius of Ti^{4+} is smaller than Fe^{3+} (Ti^{4+}: 0.605 Å, Fe^{3+}: 0.645 Å). Thus, La and Ti-codoping of BFO-based system can improve the symmetry and phase stability.

Due to the differences in electronegativity and ionic radii of the involved atoms, both bond angle and bond length between cations and anions might be changed by the doping. For localized-electron antiferromagnet of $A^{3+}FeO_3$, Néel temperature is expected to decrease with decreasing orbital overlap integral, while the e_g and t_{2g} orbital overlap integral are dependent on bond angle and bond length in a complex way. In the perovskite structured ferrite, the e_g orbit plays a crucial role for T_N.[48] Substitution of Fe ions with nonmagnetic Ti^{4+} ions would reduce the exchange interaction between adjacent magnetic moments, leading to the decrease of magnetization in doped BFO. Moreover, the substitution of Ti for Fe has an influence on the e_g and t_{2g} orbital overlapping.[16] Thus, the substitution of Fe ions with nonmagnetic Ti^{4+} ions is responsible for the shrinking of Néel temperature. In addition, the formed impurity phase and related defects may also affect the distribution of e_g and t_{2g} orbits, fermi level position, etc. A complex mechanism induced by the variation of bond length, bond angle, and the exchange interaction between adjacent magnetic moments could substantially contribute to the change of Néel temperature.

IV. SUMMARY

To summarize, composition dependence of the complex dielectric functions and electronic band transitions for $Bi_{1-x}La_xFe_{1-y}Ti_yO_3$ ceramics ($0.02 \leq x \leq 0.10$, $0.01 \leq y \leq 0.06$) have been investigated by spectroscopy ellipsometry in the temperature range of -70–$450\,^{\circ}$C. A red-shift pattern of four interband transitions with increasing the temperature is attributed to lattice thermal expansion and electron-phonon interaction. The anomalies in interband transition energies in the vicinity of T_N may be related to the coupling between magnetic and ferroelectric order parameters and spin-lattice coupling in multiferroic materials. The anomalies of partial spectral weight around T_N are also observed, suggesting the interplay between spin, charge, and orbital correlations. The Néel temperature of BLFTO ceramics decreases from 364 to $349\,^{\circ}$C with increasing doping compositions of La and Ti. The codoping of La and Ti has an influence on bond length and bond angle between cations and anions, which further leads to the modification of electronic band structure and magnetic orders. It can be confirmed that spectroscopic ellipsometry is an effective means to study phase transition of multiferroic materials.

[1]R. Haumont, I. A. Kornev, S. Lisenkov, L. Kreisel, and B. Dkhil, Phys. Rev. B. **78**, 134108 (2008).
[2]R. V. Pisarev, A. S. Moskvin, A. M. Kalashnikova, and Th. Rasing, Phys. Rev. B. **79**, 235128 (2009).
[3]I. A. Kornev, S. Lisenkov, R. Haumonnt, B. Dkhil, and L. Bellaiche, Phys. Rev. Lett. **99**, 227602 (2007).
[4]Y. F. Cui, Y. G. Zhao, L. B. Luo, J. J. Yang, H. Chang, M. H. Zhu, D. Xie, and T. L. Ren, Appl. Phys. Lett. **97**, 222904 (2010).
[5]D. Lebeugle, D. Colson, A. Forget, M. Viret, P. Bonville, J. F. Marucco, and S. Fusil, Phys. Rev. B. **76**, 024116 (2007).
[6]W. Eerenstein, N. D. Mathur, and J. F. Scott, Nature (London) **442**, 759 (2006).
[7]Z. V. Gabbasova, M. D. Kuz'min, A. K. Zvezdin, I. S. Dubenko, V. A. Murashov, and D. N. Rakov, Phys. Lett. A **158**, 491 (1991).
[8]G. Le. Bras, D. Colson, A. Forget, N. Genand-Riondet, R. Tourbot, and P. Bonvile, Phys. Rev. B **80**, 134417 (2009).
[9]D. H. Wang, W. C. Goh, M. Ning, and C. K. Ong, Appl. Phys. Lett. **88**, 212907 (2006).
[10]Z. X. Cheng, X. L. Wang, and S. X. Dou, Phys. Rev. B **77**, 092101 (2008).
[11]Yu. F. Popov, A. K. Zvezdin, G. P. Vorob'sev, A. M. Kadomtseva, V. A. Murashev, and D. N. Rakov, JETP Lett. **57**, 69 (1993).
[12]X. Qi, J. Dho, R. Tomov, M. G. Blamire, and J. L. MacManus-Driscoll, Appl. Phys. Lett. **86**, 062903 (2005).
[13]V. R. Palkar, K. G. Kumara, and S. K. Malik, Appl. Phys. Lett. **84**, 2856 (2004).
[14]J. Wang, J. B. Neaton, H. Zheng, V. Nagaraian, S. B. Ogale, B. Liu, D. Viehland, V. Vaithyanathan, D. G. Schlom, U. V. Waghmare, N. A. Spaldin, K. M. Rabe, M. Wuttig, and R. Ramesh, Science **299**, 1719 (2003).
[15]D. Lee, M. G. Kim, S. Ryu, and H. M. Jang, Appl. Phys. Lett. **86**, 222903 (2005).
[16]Y. Wang and C. W. Nan, Appl. Phys. Lett. **89**, 052903 (2006).
[17]J. H. Lee, H. J. Choi, D. Lee, M. G. Kim, C. W. Bark, S. Ryu, M. A. Oak, and H. M. Jang, Phys. Rev. B **82**, 045113 (2010).
[18]C. C. Lee and J. M. Wu, Electrochem. Solid-State Lett. **10**, G58 (2007).
[19]J. G. Wu and J. Wang, J. Am. Ceram. Soc. **93**, 2113 (2010).
[20]S. G. Choi, R. Chen, C. Persson, T. J. Kim, S. Y. Hwang, Y. D. Kim, and L. M. Mansfield, Appl. Phys. Lett. **101**, 261903 (2012).
[21]J. J. Zhu, W. W. Li, G. S. Xu, K. Jiang, Z. G. Hu, M. Zhu, and J. H. Chu, Appl. Phys. Lett. **98**, 091913 (2011).
[22]X. Chen, K. Jiang, Z. G. Hu, X. F. Chen, G. S. Wang, X. L. Dong, and J. H. Chu, Appl. Phys. Lett. **101**, 011914 (2012).

[23]X. L. Zhang, Z. G. Hu, G. S. Xu, J. J. Zhu, Y. W. Li, Z. Q. Zhu, and J. H. Chu, Appl. Phys. Lett. **103**, 051902 (2013).

[24]B. Berini, A. Fouchet, E. Popova, J. Scola, Y. Dumont, N. Franco, R. M. C. da Silva, and N. Keller, J. Appl. Phys. **111**, 053923 (2012).

[25]M. Nazari, Y. Zhao, V. V. Kuryatkov, Z. Y. Fan, A. A. Bernussi, and M. Holtz, Phys. Rev. B **87**, 035142 (2013).

[26]M. Tyunina, A. Dejneka, D. Chvostova, J. Levoska, M. Plekh, and L. Jastrabik, Phys. Rev. B **86**, 224105 (2012).

[27]Z. H. Duan, Z. G. Hu, K. Jiang, Y. W. Li, G. S. Wang, X. L. Dong, and J. H. Chu, Appl. Phys. Lett. **102**, 151908 (2013).

[28]P. K. Wang, J. P. Ansermet, S. L. Rudaz, Z. Y. Wang, S. Shore, C. P. Slichter, and J. H. Sinfelt, Science **234**, 35 (1986).

[29]Z. Salman, R. F. Kiefl, K. H. Chow, M. D. Hossain, T. A. Keeler, S. R. Kreitzman, C. D. P. Levy, R. I. Miller, T. J. Parolin, M. R. Pearson, H. Saadaoui, J. D. Schultz, M. Smadella, D. Wang, and W. A. MacFarlane, Phys. Rev. Lett. **96**, 147601 (2006).

[30]E. D. Mishina, T. V. Shersytuk, V. V. Lemanov, A. I. Morozov, A. S. Sigov, and Th. Rasing, Phys. Rev. Lett. **85**, 3664 (2000).

[31]A. Dejneka, I. Aulika, V. Trepakov, J. Krepelka, L. Jastrabik, Z. Hubicka, and A. Lynnyk, Opt. Express **17**, 14322 (2009).

[32]R. M. A. Azzam and N. M. Bashara, *Ellipsometry and Polarized Light* (Elsevier Science, New York, 1987).

[33]Y. H. Lin, Q. H. Jiang, Y. Wang, L. Chen, J. Yu, and C. W. Nan, Appl. Phys. Lett. **90**, 172507 (2007).

[34]R. Sæterli, S. M. Selbach, P. Ravindram, T. Grande, and R. Holmestad, Phys. Rev. B **82**, 064102 (2010).

[35]S. G. Choi, H. T. Yi, S. W. Cheong, J. N. Hilfiker, R. France, and A. G. Norman, Phys. Rev. B **83**, 100101 (2011).

[36]P. Lautenschlager, M. Garriga, S. Logothetidis, and M. Cardona, Phys. Rev. B **35**, 9174–9189 (1987).

[37]H. Wang, Y. Zheng, M. Q. Cai, H. T. Huang, and H. L. W. Chan, Solid State Commun. **149**, 641–644 (2009).

[38]J. B. Neaton, C. Ederer, U. V. Waghmare, N. A. Spaldin, and K. M. Rabe, Phys. Rev. B **71**, 014113 (2005).

[39]P. Ravindran, R. Vidya, A. Kjekasus, and H. Fjellvåg, Phys. Rev. B **74**, 224412 (2006).

[40]S. J. Clark and J. Robertson, Appl. Phys. Lett. **90**, 132903 (2007).

[41]W. W. Li, J. J. Zhu, J. D. Wu, J. Gan, Z. G. Hu, M. Zhu, and J. H. Chu, Appl. Phys. Lett. **97**, 121102 (2010).

[42]C. Ederer and N. A. Spaldin, Phys. Rev. B **71**, 060401 (2005).

[43]C. Y. Lan, Y. W. Jiang, and S. G. Yang, J. Mater. Sci. **46**, 734–738 (2011).

[44]R. Haumont, J. Kreisel, P. Bouvier, and F. Hippert, Phys. Rev. B **73**, 132101 (2006).

[45]M. A. Majidi, E. Thoeng, P. K. Gogoi, F. Wendt, S. H. Wang, I. Santoso, T. C. Asmara, I. P. Handayani, P. H. M. van Loosdrecht, A. A. Nugroho, M. Rübhausen, and A. Rusydi, Phys. Rev. B **87**, 235135 (2013).

[46]J. Kunze, S. Naler, J. Bäckström, M. Rübhausen, and J. F. Mitchell, Phys. Rev. B **67**, 134417 (2003).

[47]K. Tobe, T. Kimura, Y. Okimoto, and Y. Tokura, Phys. Rev. B **64**, 184421 (2001).

[48]J. B. Goodenough, Phys. Rev. **164**, 785 (1967).